



**HAL**  
open science

## Silicon electrodeposition in molten fluorides

Anne-Laure Bieber, Laurent Massot, Mathieu Gibilaro, Laurent Cassayre,  
Pierre Taxil, Pierre Chamelot

► **To cite this version:**

Anne-Laure Bieber, Laurent Massot, Mathieu Gibilaro, Laurent Cassayre, Pierre Taxil, et al.. Silicon electrodeposition in molten fluorides. *Electrochimica Acta*, 2011, 62, pp.282-289. 10.1016/j.electacta.2011.12.039 . hal-03537607

**HAL Id: hal-03537607**

**<https://hal.science/hal-03537607>**

Submitted on 20 Jan 2022

**HAL** is a multi-disciplinary open access archive for the deposit and dissemination of scientific research documents, whether they are published or not. The documents may come from teaching and research institutions in France or abroad, or from public or private research centers.

L'archive ouverte pluridisciplinaire **HAL**, est destinée au dépôt et à la diffusion de documents scientifiques de niveau recherche, publiés ou non, émanant des établissements d'enseignement et de recherche français ou étrangers, des laboratoires publics ou privés.



## Open Archive Toulouse Archive Ouverte (OATAO)

OATAO is an open access repository that collects the work of Toulouse researchers and makes it freely available over the web where possible.

This is an author-deposited version published in: [www.aaa.comhttp://oatao.univ-toulouse.fr/](http://www.aaa.comhttp://oatao.univ-toulouse.fr/)  
Eprints ID: 8619

**To link to this article:** DOI:10.1016/j.electacta.2011.12.039  
<http://dx.doi.org/10.1016/j.electacta.2011.12.039>

**To cite this version:**

Bieber, Anne-Laure and Massot, Laurent and Gibilaro, Mathieu and Cassayre, Laurent and Taxil, Pierre and Chamelot, Pierre *Silicon electrodeposition in molten fluorides*. (2011) *Electrochimica Acta*, vol. 62 . pp. 282-289. ISSN 0013-4686

Any correspondence concerning this service should be sent to the repository administrator:  
[staff-oatao@inp-toulouse.fr](mailto:staff-oatao@inp-toulouse.fr)

# Silicon electrodeposition in molten fluorides

A.L. Bieber, L. Massot\*, M. Gibilaro, L. Cassayre, P. Taxil, P. Chamelot

Université de Toulouse; INPT, UPS, CNRS; Laboratoire de Génie Chimique; 118 Route de Narbonne, F-31062 Toulouse, France

## A B S T R A C T

Silicon nucleation process was investigated in molten NaF–KF (40–60 mol%) on silver electrodes in the 820–950 °C temperature range in order to optimize silicon coating operating conditions. Chronoamperometric measurements evidenced that silicon electrodeposition process involved an instantaneous nucleation with diffusion-controlled nuclei growth whatever temperature and Si(IV) ions concentration in the mixture. The overpotential and temperature influence on nucleation sites number was also studied.

Silicon deposits were obtained using the same temperature range as nucleation study, for different current densities on substrates: Ni, Ag, C<sub>graphite</sub> and C<sub>vitreous</sub>. A sensitive influence of the cathodic substrate on the deposit adherence and roughness was observed and discussed.

## Keywords:

Instantaneous nucleation

Silicon

Electrodeposition

Molten fluorides

Chronoamperometry

## 1. Introduction

Photovoltaic technology is emerging as a major source of electrical energy [1], and the most common base material for photovoltaic cell is solar grade silicon (SoG-Si). Due to a constantly growing demand for SoG-Si, the development of new processes allowing the production of cheap SoG-Si is a main issue for the solar energy industry.

In the 1980s, silicon electrodeposition in molten salts has been considered as an attractive option for SoG-Si production [2]. Indeed, silicon metal is more reductive than hydrogen meaning that silicon electrodeposition has to be carried out in non-aqueous electrolytes such as alkali metal halides. However, no electrolytic Si production process has found commercial application up to now. Considering more recent concerns about carbon-free energy production and growing needs for SoG-Si, such kind of process is nevertheless being reassessed, and, for that purpose, basic investigations on the salts properties, Si(IV) reduction mechanism and silicon deposition strategies are needed.

In the frame of a production route based on electrorefining (either from MG-Si or from Si cutting remains [3]), it was decided to focus on the electrodeposition process of dissolved Si(IV) in molten fluoride. The main objective was to evaluate the feasibility of such reaction and to provide an academic study of the Si(IV) reduction reaction, thanks to specific electrochemical techniques [4,5]. At this

point of the study, the purity of the obtained deposits was not considered as an issue.

It was shown, in a previous work [6], that the volatility of Si(IV) compounds greatly depends on the nature of the fluoride mixture. The NaF–KF eutectic mixture, which highly stabilizes Si(IV) compounds, was thus selected as the electrolyte for the present study.

The article describes a next stage in the preparation of silicon layers for solar energy which is the demonstration of the electrolysis technique validity in molten salts technique to recover pure silicon on a cathode.

For this purpose, the nucleation process and the silicon nuclei growth on silver are investigated using cyclic voltammetry and chronoamperometry and these results are compared with suitable models [4,7] in order to state whether the nucleation is instantaneous or progressive. Meanwhile, the overvoltage and temperature influence on the nucleation mode and nucleation sites number were examined. Then, silicon deposition runs were carried with various electrode substrates (Ni, Ag, C<sub>graphite</sub> and C<sub>vitreous</sub>), current densities (–20 to –200 mA cm<sup>–2</sup> range) and temperatures (820–900 °C range). The influence of each parameter on the coating adherence and roughness was observed by scanning electron microscopy (SEM).

## 2. Experimental

### 2.1. Cell

The cell was a vitreous carbon crucible placed in a cylindrical vessel made of refractory steel and closed by a stainless steel lid cooled by circulating water. The description of this cell has been

\* Corresponding author. Tel.: +33 561558194; fax: +33 561556139.  
E-mail address: massot@chimie.ups-tlse.fr (L. Massot).

detailed in previous work [8]. The experiments were performed under an inert argon atmosphere (Linde). The cell was heated using a programmable furnace and the temperature was measured using a chromel–alumel thermocouple.

The electrolytic bath consisted of the NaF–KF (40–60 mol%) eutectic mixture (Carlo Erba 99.995%). As mentioned earlier, the choice of this specific solvent was based on its stabilizing properties regarding to the volatility of Si(IV) compounds [6]. The mixture was initially dehydrated by heating under vacuum ( $7 \times 10^{-2}$  mbar) from ambient temperature up to its melting point during one week. Silicon ions were introduced into the bath in the form of sodium hexafluorosilicate  $\text{Na}_2\text{SiF}_6$  (Alfa Aesar 99.99%) powder.

## 2.2. Electrodes

Silver wires (1 mm diameter), vitreous and graphite carbon rods (3 mm diameter–Mersen spectroscopic quality) and nickel plates (50 mm  $\times$  10 mm  $\times$  1 mm) were used as working electrode. The surface area of the working electrode was determined after each experiment by measuring the immersion depth in the bath. The auxiliary electrode was a silicon thick plate (4 mm  $\times$  8 mm  $\times$  11 mm) with a large surface area (3 cm<sup>2</sup>). The potentials were measured with reference to a silicon plate immersed in the molten electrolyte.

## 2.3. Techniques

The electrochemical techniques used for the silicon nucleation and deposition investigation were cyclic voltammetry and chronoamperometry. All the electrochemical measurements were performed with an AutolabPGStat 30 potentiostat/galvanostat controlled by a computer using the research software GPES.

The silicon deposits were observed by SEM coupled with EDX probe, after cleaning in a HCl–AlCl<sub>3</sub>–H<sub>2</sub>O mixture at 50 °C with ultrasonic waves.

## 3. Results and discussion

### 3.1. Si(IV) ions reduction mechanism

The silicon ions reduction in fluorides media was found to be a single step process exchanging 4 electrons (as already presented in Ref. [6]):



Cyclic voltammetry was carried out on a silver electrode in NaF–KF–Na<sub>2</sub>SiF<sub>6</sub> system in the 820–950 °C temperature range. Fig. 1 presents a typical cyclic voltammogram of the NaF–KF–Na<sub>2</sub>SiF<sub>6</sub> (0.24 mol kg<sup>-1</sup>) system at 850 °C on silicon electrode. This cyclic voltammogram exhibits only one reduction peak at –0.15 V vs Si and its associated reoxidation peak at 0.15 V vs Si. The linear relationship between Si(IV) reduction peak intensity and the square root of the scan rate has been verified (see the inset of Fig. 1), proving that the electrochemical reduction process is controlled by the Si(IV) ions diffusion in the bath (Berzins–Delahay [9] valid for a reversible soluble/insoluble system):

$$I_p = -0.61nFSc^0 \left( \frac{nFD}{RT} \right)^{1/2} \nu^{1/2} \quad (2)$$

where  $n$  is the number of exchanged electrons,  $F$  is the Faraday's constant (C mol<sup>-1</sup>),  $S$  is the electrode surface area (m<sup>2</sup>),  $c^0$  is the solute concentration (mol m<sup>-3</sup>),  $D$  is the diffusion coefficient (m<sup>2</sup> s<sup>-1</sup>),  $T$  is the temperature (K) and  $\nu$  is the potential scan rate (V s<sup>-1</sup>).

Furthermore, the diffusion coefficient  $D$  can be calculated using Eq. (2) and the results obtained from the inset of Fig. 1. At the temperature of 850 °C, its value is  $2.9 \times 10^{-9}$  m<sup>2</sup> s<sup>-1</sup>. The temperature dependence of the diffusion coefficient, in the 820–950 °C temperature range, is given in Eq. (3):

$$D = 1.13 \times 10^{-5} \exp \left( -\frac{77.2 \times 10^3}{RT} \right) \quad (3)$$

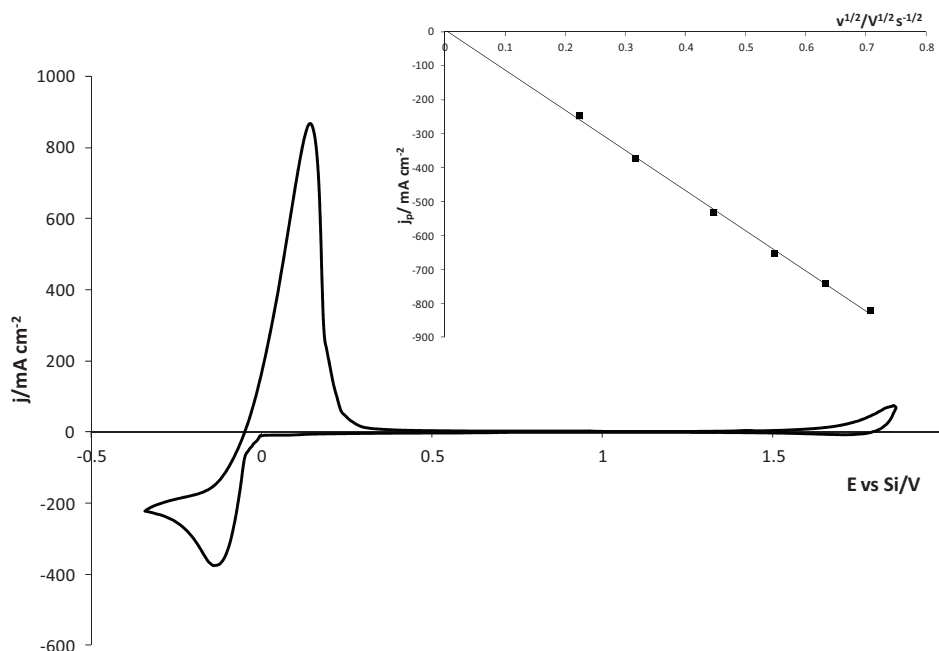


**Fig. 1.** Cyclic voltammogram of NaF–KF–Na<sub>2</sub>SiF<sub>6</sub> ( $c_0 = 0.24$  mol kg<sup>-1</sup>) at 850 °C; working electrode: Ag; auxiliary electrode: Si; reference electrode: Si; Scan rate = 100 mV s<sup>-1</sup>/Inset: Linear relationship of Si(IV) reduction peak current density versus the square root of the scanning potential rate.

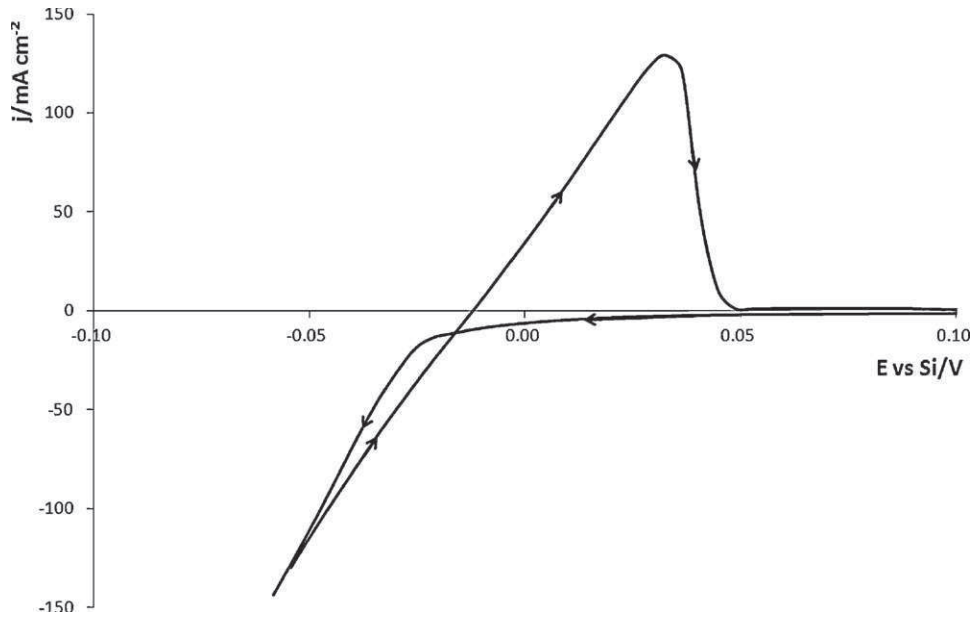


**Fig. 2.** Cyclic voltammogram highlighting the nucleation cross-over for silicon deposition in NaF–KF–Na<sub>2</sub>SiF<sub>6</sub> ( $c_0 = 0.24 \text{ mol kg}^{-1}$ ) at 850 °C; working electrode: Ag ( $S = 0.31 \text{ cm}^2$ ); auxiliary electrode: Si; reference electrode: Si; Scan rate =  $50 \text{ mV s}^{-1}$ .

where  $D$  is the diffusion coefficient ( $\text{m}^2 \text{ s}^{-1}$ ) and  $T$  the temperature (K).

### 3.2. Silicon electrocrystallisation process

#### 3.2.1. Cyclic voltammetry

Fig. 2 shows a cyclic voltammogram where the cathodic limit potential is higher than the Si(IV) ions reduction peak potential observed on Fig. 1. This figure highlights the main features of an electrocrystallisation process:

- The observation of a cross-over of direct and reverse scanning curves, which is the consequence of the irreversible nucleation step during the reduction scan [9,10].
- The asymmetrical shape of the reoxidation peak, typical of the redissolution of a solid phase deposited during the cathodic run (stripping peak).
- The low cathodic background current observed between 0.02 V/Si and  $-0.03 \text{ V/Si}$  can be attributed to the formation of dissolved silicon into the cathodic substrate (Ag).

#### 3.2.2. Chronoamperometry

According to previous works in molten salts [11,12], chronoamperometry is a suitable technique to investigate nucleation phenomena. The transient curves shape ( $I = f(t)$ ) at the beginning of the cathodic polarization allows to determine the nuclei formation mode, growth and geometry [7,13,14]. A series of chronoamperograms are presented in Fig. 3, at different overvoltages on silver electrode, in NaF–KF–Na<sub>2</sub>SiF<sub>6</sub> ( $c_0 = 0.24 \text{ mol kg}^{-1}$ ), at 850 °C. This technique was not found suitable for nucleation studies on carbon substrates, since this element alloys with silicon at the first stage of the Si electrodeposition according to the binary diagram [15].

The curves are divided into three parts (cf. inset of Fig. 3):

- Part I: During this part, corresponding to the double-layer charging, the first nuclei form on the electrode. The time dependence on the number of nuclei generated is given by the Poisson's law [7]:

$$N = N_0(1 - e^{-At}) \quad (4)$$

where  $N$  is the nuclei density ( $\text{cm}^{-2}$ ),  $N_0$  the total number of nucleation sites ( $\text{cm}^{-2}$ ),  $A$  the nucleation constant for a site ( $\text{s}^{-1}$ ) and  $t$  the time (s).

- If the value of  $A$  is high, thus  $N = N_0$  and the nucleation is instantaneous meaning that all the nuclei appear at the beginning of the polarization.
- For low values of  $A$ ,  $N = AN_0t$ , meaning that the nucleation is progressive.

- Part II: The current rises, due to an active surface area increase, owing to the nuclei growth. Correlatively, the electrolyte diffusion promotes the current decrease. The competition between these two effects leads to a maximum peak intensity and its coordinates ( $t_m$ ;  $I_m$ ) are used for the nucleation modeling. For short times, the current in this second part allows the nucleation mode determination and obeys the following relation according to [7]:

$$j = \alpha t^x \quad (5)$$

where  $\alpha$  and  $x$  depend on the growth control, the nuclei geometry and the nucleation mode. In the case of hemispherical 3D nucleation limited by diffusion,  $x$  is equal to  $1/2$  or  $3/2$  for instantaneous or progressive nucleation respectively. Eq. (5) has been plotted in Fig. 4 and the proportionality between  $j$  and  $t^{1/2}$  evidences that an instantaneous silicon nucleation occurs.

- Part III: Si(IV) ions diffusion control is predominant, and a slow current decrease is observed following the Cottrell's law [8,9], which implies a linear relationship between current and  $t^{-1/2}$ . Scharifker and Hills [7] established a model based on a dimensional intensity and time:  $(I/I_m)^2 = f(t/t_m)$ . For an instantaneous nucleation, the curve parameters are described by the Eqs. (6)–(9) as:

$$\left(\frac{I}{I_m}\right)^2 = \frac{1.9542}{t/t_m} \left\{ 1 - \exp \left[ -1.2564 \left(\frac{t}{t_m}\right) \right] \right\}^2 \quad (6)$$

with

$$t_m = \frac{1.2564}{N_0 \pi k D} \quad k = \left(\frac{8c_0 M \pi}{\rho}\right)^{1/2} \quad (7)$$

and

$$I_m = 0.6382 n F D c_0 (k N_0)^{1/2} \quad (8)$$

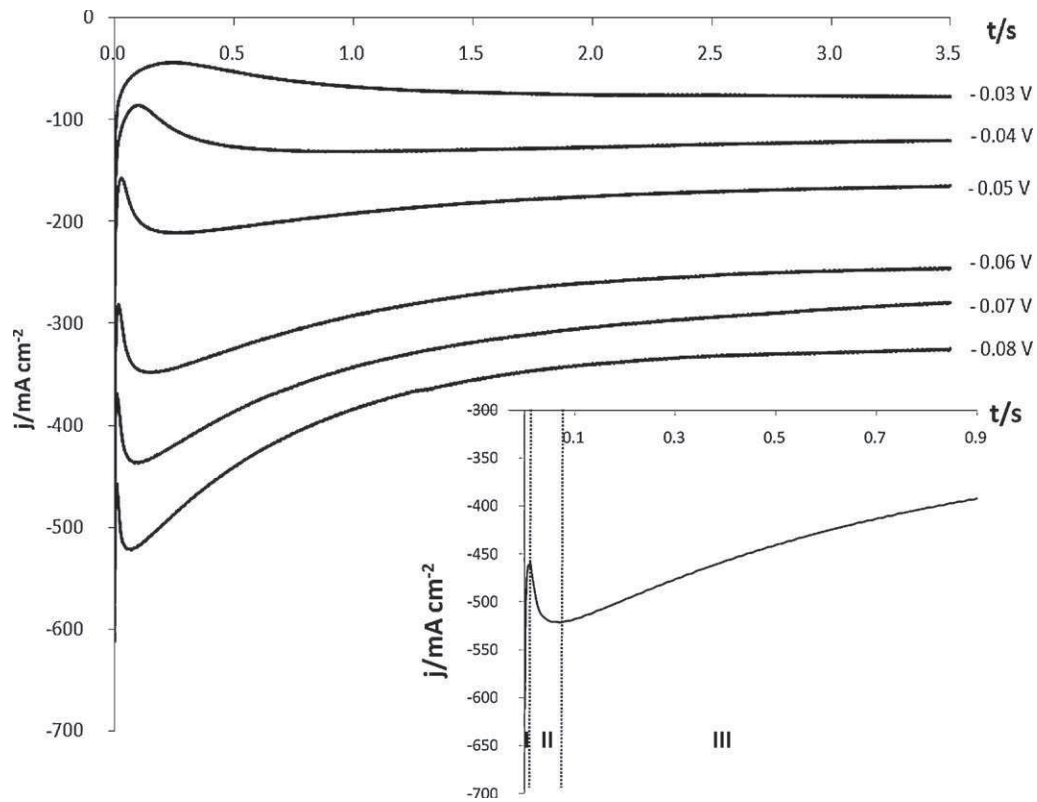


**Fig. 3.** Chronoamperograms on silver electrode at various overvoltages in NaF–KF–Na<sub>2</sub>SiF<sub>6</sub> ( $c_0 = 0.24 \text{ mol kg}^{-1}$ ) at 850 °C; auxiliary electrode: Si; reference electrode: Si/Inset: Chronoamperogram on silver electrode at  $\eta = -0.04 \text{ V}$  in NaF–KF–Na<sub>2</sub>SiF<sub>6</sub> ( $c_0 = 0.24 \text{ mol kg}^{-1}$ ) at 850 °C.

$$I_m^2 t_m = 0.1629(nFc_0)^2 D \quad (9)$$

where  $n$  is the number of exchanged electrons,  $F$  the Faraday's constant ( $\text{C mol}^{-1}$ ),  $c_0$  the solute concentration ( $\text{mol m}^{-3}$ ),  $M$  the molar mass ( $\text{kg mol}^{-1}$ ),  $\rho$  the density ( $\text{kg m}^{-3}$ ) and  $D$  the diffusion coefficient ( $\text{m}^2 \text{ s}^{-1}$ ).

Using the chronoamperograms at different temperatures, the experimental curves  $(I/I_m)^2 = f(t/t_m)$  are compared to the theoretical ones in Fig. 5.

The experimental data are in agreement with Eq. (6), proving that the instantaneous nucleation mode is predominant at the considered temperature, overvoltage and concentration range. Based on SEM observations, similar conclusions were obtained by

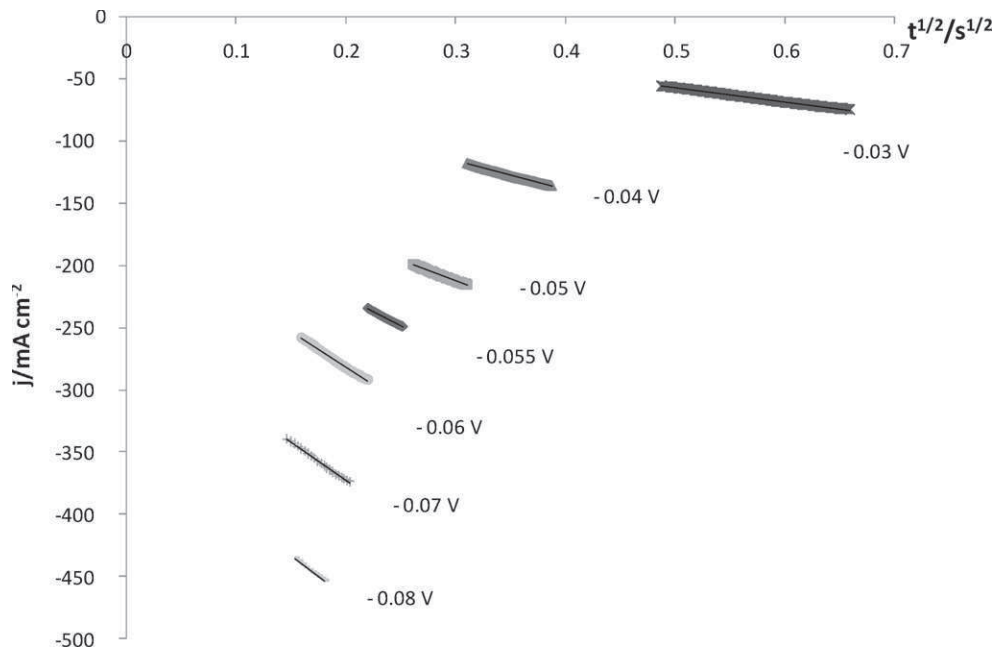


**Fig. 4.** Plottings of  $j = f(t^{1/2})$  of the chronoamperogram second part at various overvoltages in NaF–KF–Na<sub>2</sub>SiF<sub>6</sub> ( $c_0 = 0.24 \text{ mol kg}^{-1}$ ) at 850 °C; working electrode: Ag; auxiliary electrode: Si; reference electrode: Si.

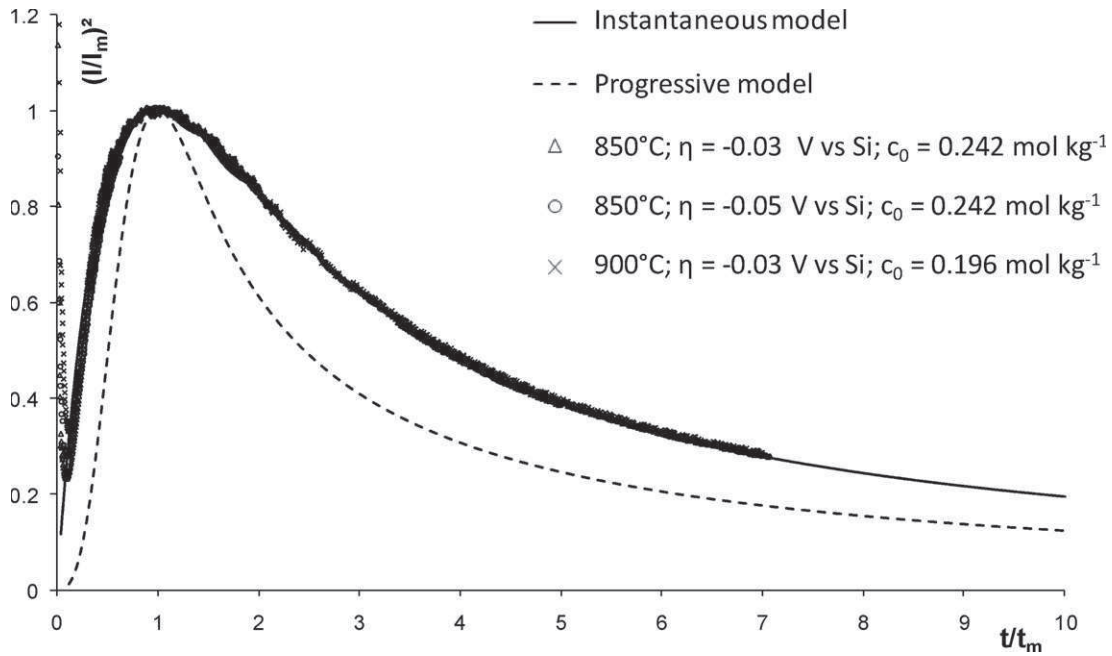


**Fig. 5.** Comparison of the dimensionless experimental data at various temperatures with the theoretical models in NaF–KF–Na<sub>2</sub>SiF<sub>6</sub>; working electrode: Ag; auxiliary electrode: Si; reference electrode: Si.

Carleton et al. for the silicon nucleation mode on vitreous carbon in LiF–KF–K<sub>2</sub>SiF<sub>6</sub> at 750 °C [16]. The SEM micrograph of nuclei, presented in Fig. 6 ( $t = 1.1$  s and  $\eta = -0.04$  V vs Si), seems to confirm the instantaneous nucleation mode and the hemispherical geometry of germs.

The nucleation sites number  $N_0$  were calculated using Eqs. (6) and (8) at various overvoltages and temperatures; the values are gathered in Table 1.

An increase in the nucleation sites number with the overvoltage is observed while the product  $I_m^2 t_m$  remains constant, as foreseen in Eq. (9). As previously demonstrated in Section 3.1, the nuclei growth is limited by Si(IV) ions diffusion, which is either hemispherical or linear. In linear diffusion, the slope  $\alpha$  (defined in Eq.

**Table 1**

Overvoltage influence on the nuclei favourable sites number in NaF–KF–Na<sub>2</sub>SiF<sub>6</sub> ( $c_0 = 0.24$  mol kg<sup>-1</sup>) at 850 °C; working electrode: Ag; auxiliary electrode: Si; reference electrode: Si.

$\eta$ (V)	$i_m$ (A cm <sup>-2</sup> )	$t_m$ (s)	$10^{-2} i_m^2 t_m$	$10^{-11} N_0$
-0.030	-0.098	1.55	1.49	2.10
-0.040	-0.158	0.680	1.70	4.79
-0.050	-0.236	0.298	1.66	10.9
-0.055	-0.274	0.218	1.64	14.9
-0.060	-0.316	0.167	1.66	19.5
-0.070	-0.393	0.116	1.79	28.1
-0.080	-0.469	0.076	1.67	42.8

(5)) follows Eq. (10) whereas the Eq. (11) describes a hemispherical diffusion:

$$\alpha = -8nFM^2c_0^3N_0D^{3/2}\rho^{-2}\pi^{-1/2} \quad (10)$$

$$a = -nF\pi N_0(2Dc_0)^{3/2}\left(\frac{M}{\rho}\right)^{1/2} \quad (11)$$

The  $N_0$  values, reported in Table 1, are compared in Table 2 with the one calculated from the slopes of  $j = f(t^{-1/2})$  (Fig. 4) in each different diffusion conditions, derived from Eqs. (10) and (11).

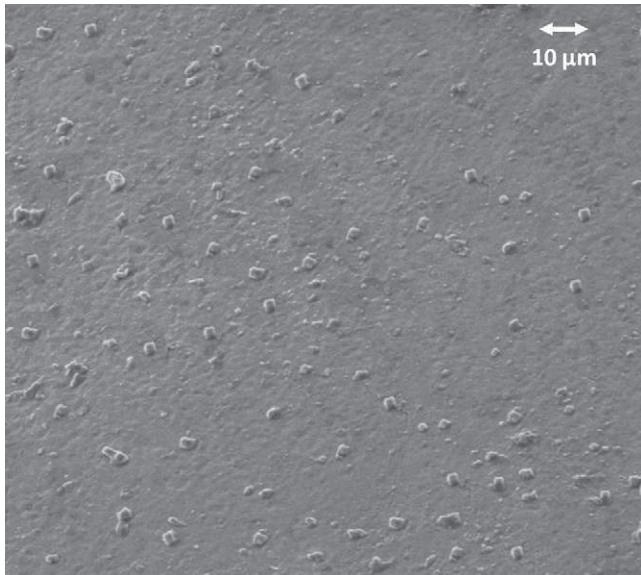
For the values mentioned in Table 2, this comparison seems to state that the nuclei's growth is governed by a linear diffusion and thus should lead to a dendritic growth.

Table 3 shows the temperature influence for silicon nucleation on a silver electrode at various overvoltages. It indicates that the nucleation sites number  $N_0$  increases significantly with both

**Table 2**

Comparison of the nuclei favourable sites number in NaF–KF–Na<sub>2</sub>SiF<sub>6</sub> ( $c_0 = 0.24$  mol kg<sup>-1</sup>) at 850 °C for different diffusion models; working electrode: Ag; auxiliary electrode: Si; reference electrode: Si.

$\eta$ (V)	$10^{-11} N_0$	Linear diffusion Eq. (10) $10^{-11} N_0$	Hemispherical diffusion Eq. (11) $10^{-8} N_0$
-0.03	2.10	2.14	0.47
-0.04	4.79	4.44	0.98
-0.05	10.9	6.49	1.44



**Fig. 6.** SEM micrograph of silicon nuclei on silver electrode in NaF–KF–Na<sub>2</sub>SiF<sub>6</sub> ( $c_0 = 0.24$  mol kg<sup>-1</sup>) at 850 °C;  $\eta = -0.04$  V vs Si;  $t = 1.1$  s.

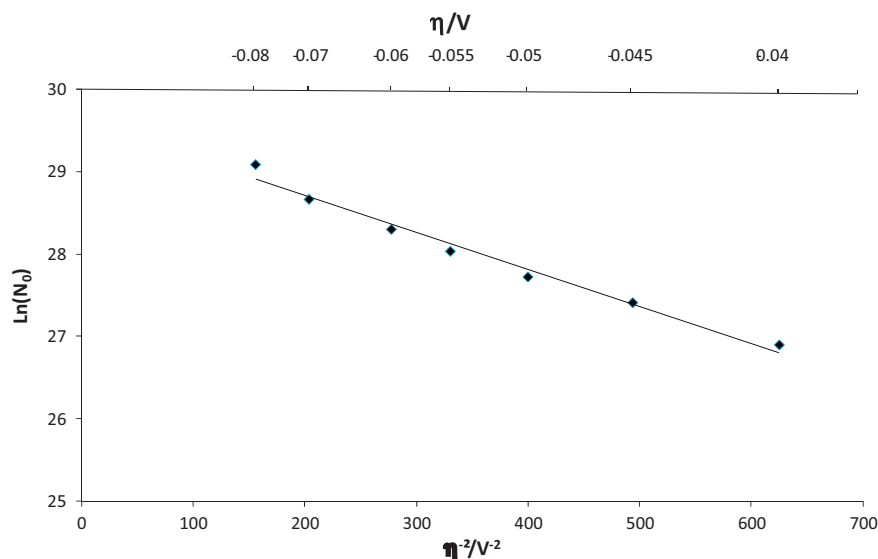


**Fig. 7.** Linear relationship between the logarithm of the nucleation favourable sites number and square overvoltage inverse in NaF–KF–Na<sub>2</sub>SiF<sub>6</sub> ( $c_0 = 0.24 \text{ mol kg}^{-1}$ ) at 850 °C; working electrode: Ag; auxiliary electrode: Si; reference electrode: Si.

temperature and overvoltage. In Fig. 7, a linear relationship is evidenced between  $\ln(N_0)$  and the inverse of square overvoltage and obeys Eq. (12) [13,17]:

$$\ln(N_0) = A - \frac{B}{\eta^2} \quad (12)$$

Knowing the nucleation mode, Fig. 7 allows optimized electrodeposition conditions to be proposed. Indeed, to obtain a smooth coating structure, the creation of a high number of nuclei is essential, which is favoured by both high temperatures and overvoltages. Nevertheless for high overvoltage, a too high electrolyte diffusion limitation can promote dendritic growth phenomena. Taking into account these conflicting effects, it was decided to realise silicon coatings at different overvoltages and temperatures.

### 3.3. Silicon electrodeposition

Various runs of silicon electrodeposition on different cathodic substrates were performed taking into account the conditions suggested in the previous section. The electrolyses were conducted under potentiostatic conditions as mentioned in references [16,18,19].

The current efficiency was determined on graphite and silver electrodes using the mass difference between the cathode before and after the electrolysis run. It was found to be between 88 and 96% for low current densities ( $-20$  and  $-100 \text{ mA cm}^{-2}$ ) resulting in dense deposits; at high current densities, the deposits were very dendritic and brittle, which caused silicon losses during the washing treatment: the current efficiency could not be evaluated. These current

efficiencies are higher than those obtained by Elwell and Rao [20] in LiF–KF–K<sub>2</sub>SiF<sub>6</sub> at 750 °C: 50% as an average current efficiency and 80% for  $-25 \text{ mA cm}^{-2}$  current density.

#### 3.3.1. Operating conditions dependence

Several silicon coatings were obtained in NaF–KF–Na<sub>2</sub>SiF<sub>6</sub> ( $c_0 = 0.47 \text{ mol kg}^{-1}$ ) in the 820–900 °C temperature range on carbon rod, for applied current densities between  $-20$  and  $-200 \text{ mA cm}^{-2}$ . After frozen salt removal, the coating microstructures were observed by SEM. The micrographs, presented in Fig. 8, suggest first that higher temperatures favour somewhat the surface coating regularity but also that high current densities are detrimental for this property, which is in agreement with studies from Elwell in NaF–CaF<sub>2</sub>–SiO<sub>2</sub> [19], Boen and Bouteillon in LiF–NaF–Na<sub>2</sub>SiF<sub>6</sub> [18] and also for other metals deposition, e.g. on tantalum in molten fluorides [13]. For applications where high plating rates are required, the use of pulsed current could help preventing the diffusion limitation and thus lead to more regular coatings at high current densities [21–23].

EDX analysis of the deposits did not reveal any other compound than Si that means that the deposit purity is assumed to be at least 99.9%. As for the purity of the obtained Si, which is a key issue for the solar industry, recent work from Nohira et al. [24,25] showed that, in the case of processes involving molten salts solvents at high temperatures, a careful design of the electrorefiner has to be made in order to avoid pollution from the cell elements.

#### 3.3.2. Substrate influence

Due to the strong effect of the current density on the regularity of the coating surface state and the moderate influence of the temperature, electrodeposition runs were carried out at  $-20 \text{ mA cm}^{-2}$  at 820 °C for 5 h. Fig. 9 shows SEM micrographs of silicon deposits on three electrode substrates (Ni, Ag and C<sub>v</sub>).

On nickel (a), silver substrate (b) and vitreous carbon (c), a columnar dendritic coating, a silicon microwire structure and a sponge-like structure were observed respectively. The smooth and dense deposit observed on graphite carbon at 820 °C,  $-20 \text{ mA cm}^{-2}$  (Fig. 8) is in agreement with Rao et al. work [26] in LiF–KF–K<sub>2</sub>SiF<sub>6</sub> at 750 °C. According to Carleton et al. [16], the differences between vitreous and graphite carbon are due to their different structural

**Table 3**  
Temperature influence on the nuclei favourable sites number at different overvoltages in NaF–KF–Na<sub>2</sub>SiF<sub>6</sub> ( $c_0 = 0.24 \text{ mol kg}^{-1}$ ); working electrode: Ag; auxiliary electrode: Si; reference electrode: Si.

$\eta$ (V)	$t_m$ (s)		$10^{-11}N_0$	
	850 °C	900 °C	850 °C	900 °C
-0.03	1.55	0.568	1.46	5.15
-0.04	0.680	0.336	3.41	8.70
-0.05	0.298	0.203	12.4	14.41

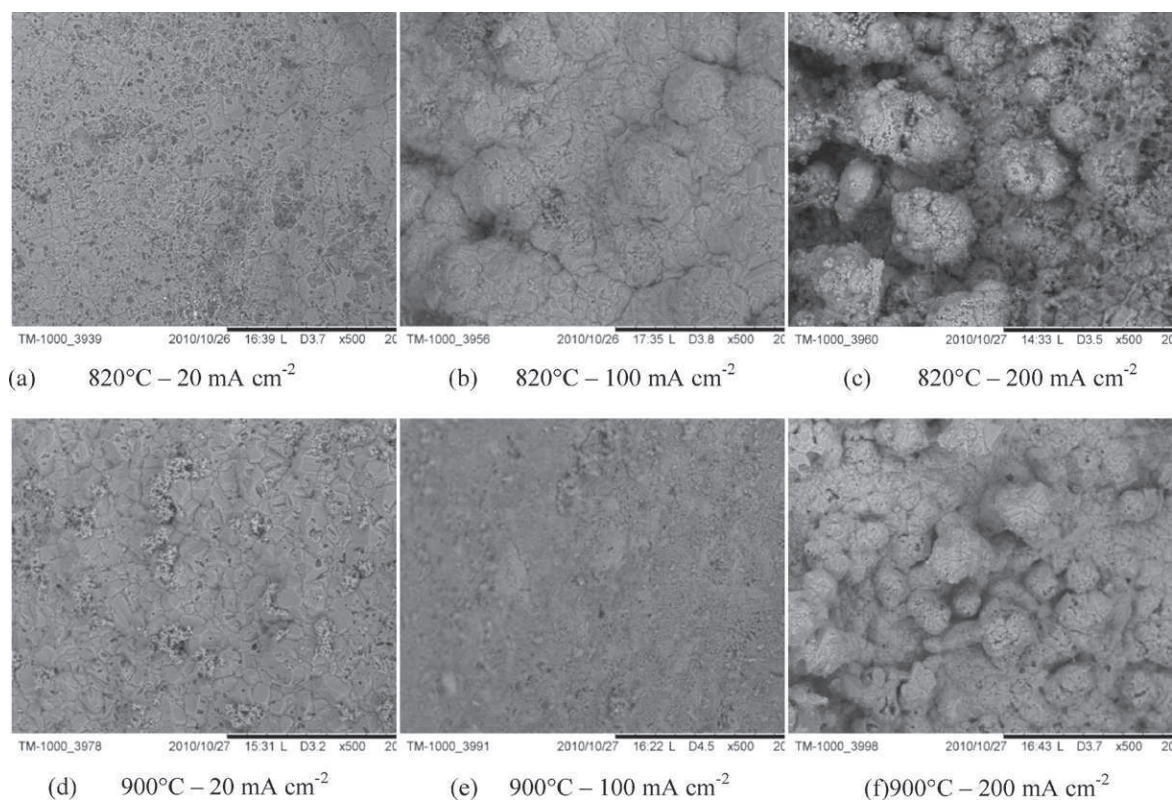


**Fig. 8.** SEM observations of silicon coatings on carbon at various current densities and temperatures.

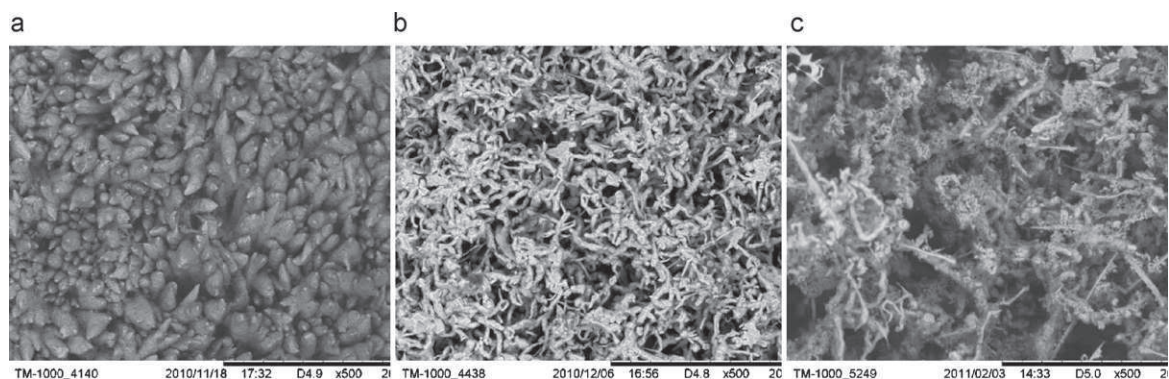
properties leading to significant differences of nucleation active sites.

Fig. 10 presents SEM observations of silicon coatings cross section on various substrates (Ni, Ag, C and C<sub>v</sub>) at  $-20 \text{ mA cm}^{-2}$  at  $820^\circ\text{C}$ .

- Nickel substrate (a): Ni–Si alloys layers are observed at the substrate-coating boundary, which seems to promote a very high adherence of the silicon deposit on the substrate. SEM-EDX analysis shows two silicide layers under the columnar layer and XRD measurement on the Ni–Si surface deposit indicates the presence of  $\text{Ni}_3\text{Si}_2$ , NiSi and Si formation. Previous works on intermetallic compounds Ni–Si preparation by high temperature solid diffusion evidenced four nickel silicides:  $\text{Ni}_5\text{Si}$ ,  $\text{Ni}_2\text{Si}$ ,  $\text{Ni}_3\text{Si}_2$ , NiSi [27,28]. Borivent et al. [27] showed that the growth of  $\text{Ni}_3\text{Si}_2$  proceeds by needles: it could explain that in the present work, the silicon coating growth over  $\text{Ni}_3\text{Si}_2$  needles is columnar,

contrary to other substrates. Our conclusion is that Ni substrate is not adapted to silicon electrodeposition due to high interdiffusion rate between the compounds which promotes the formation of intermetallic compounds instead of pure Si.

- Silver electrode (b): no alloy formation is observed, in accordance with the Ag–Si phase diagram [29]. The silicon layer, covering the Ag surface, becomes progressively more porous and filamentous and tends to break during the washing treatment.
- Graphite carbon (c): a dense SiC layer ( $\sim 10 \mu\text{m}$ ) was formed by interdiffusion between silicon deposit and carbon electrode. On this thin layer, a dense and adherent silicon layer of  $\sim 100 \mu\text{m}$  thickness was obtained. Similar results on graphite were obtained by Rao et al. who attributed the deposit compactness to the coalescence of silicon nodules in a three-dimensional growth [30].
- Vitreous carbon (d): a rough and poorly adherent deposit was obtained. This brittle deposit was most probably broken during the hot pressing carried out for the sample embedding.



**Fig. 9.** SEM observations of silicon deposit surfaces at  $-20 \text{ mA cm}^{-2}$  at  $820^\circ\text{C}$  for 5 h on various substrates: (a) nickel; (b) silver; (c) vitreous carbon.

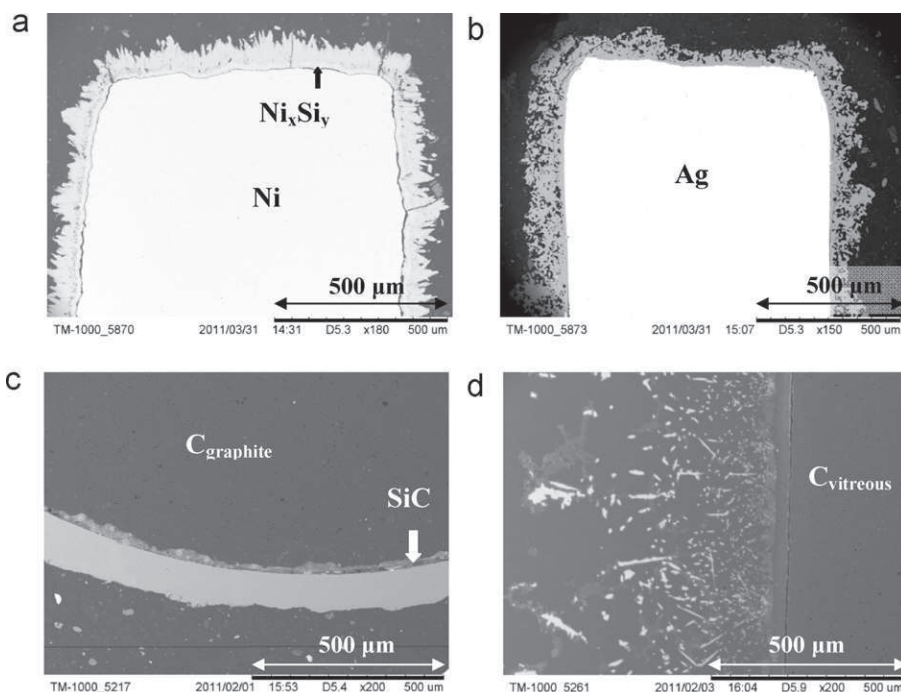


**Fig. 10.** Cross section SEM observations of silicon deposits at  $-20 \text{ mA cm}^{-2}$  at  $820^\circ\text{C}$  for 5 h on various substrates: (a) nickel; (b) silver; (c) graphite carbon; (d) vitreous carbon.

#### 4. Conclusions

The silicon nucleation mechanism was studied in a  $\text{NaF-KF-Na}_2\text{SiF}_6$  salt mixture on silver electrode, using mainly chronoamperometry: the silicon nuclei are generated instantaneously with a linear diffusion-controlled hemispherical growth. Moreover, the nucleation sites number  $N_0$  increases with the temperature and the overvoltage. Then, galvanostatic electrolyses were performed by varying temperature and current density on a carbon rod. SEM observations showed that high temperature and low current density lead to a smoother deposit, with a purity (measured by EDX) higher than 99.9%. The cathodic substrate tests ( $\text{Ni}$ ,  $\text{Ag}$ ,  $\text{C}$  and  $\text{C}_v$ ) allowed concluding that graphite carbon is a well-adapted cathodic material due to the deposit adherence and structure; on vitreous carbon, the deposits are dendritic; on silver substrate, the deposits are poorly adherent while on nickel, many alloys were formed, hindering pure silicon deposition. When the current density increases, the coating becomes rougher. At high current densities, the silicon ions diffusion limitation strongly influences the silicon growth, leading to a more dendritic deposit.

#### References

- [1] M.A. Green, *Solar Energy* 76 (2004) 3.
- [2] D. Elwell, R.S. Feigelson, *Solar Energy Mater.* 6 (1982) 123.
- [3] T. Ulset, S. Julsrud, L. Cassayre, P. Chamelot, L. Massot, P. Taxil, T.L. Naas, *PCT Int. Appl. WO 2008156372* (2008).
- [4] P. Chamelot, P. Taxil, B. Lafage, *Electrochim. Acta* 39 (17) (1994) 2571.
- [5] P. Taxil, P. Chamelot, L. Massot, C. Hamel, *J. Min. Metall. B* 39 (1-2) (2003) 177.
- [6] A.L. Bieber, L. Massot, M. Gibilaro, L. Cassayre, P. Chamelot, P. Taxil, *Electrochim. Acta* 56 (2011) 5022.
- [7] B. Scharifker, G. Hills, *Electrochim. Acta* 28 (1983) 879.
- [8] L. Massot, P. Chamelot, F. Bouyer, P. Taxil, *Electrochim. Acta* 47 (2002) 1949.
- [9] A.J. Bard, L.R. Faulkner, *Electrochemical Methods: Fundamentals and Applications*, John Wiley and Sons, New York, 2001.
- [10] X.H. Xu, C.L. Hussey, *J. Electrochem. Soc.* 139 (1992) 1295.
- [11] L. Massot, P. Chamelot, P. Palau, P. Taxil, *Electrochim. Acta* 50 (2005) 5408.
- [12] L. Massot, P. Chamelot, F. Bouyer, P. Taxil, *Electrochim. Acta* 48 (2003) 465.
- [13] P. Chamelot, B. Lafage, P. Taxil, *J. Electrochem. Soc.* 143 (5) (1996) 1570.
- [14] L. Legrand, A. Tranchand, R. Messina, *J. Electrochem. Soc.* 141 (2) (1994) 378.
- [15] R.W. Olesinski, G.J. Abbaschian, *Bull. Alloy Phase Diagrams* 5 (1984) 486.
- [16] K.L. Carleton, J.M. Olson, A. Kibbler, *J. Electrochem. Soc.* 130 (4) (1983) 782.
- [17] T. Erdey-Gruz, M. Volmer, *Z. Phys. Chem.* 157 (1931) 165.
- [18] R. Boen, J. Bouteillon, *J. Appl. Electrochem.* 13 (1983) 277.
- [19] D. Elwell, *Solar Energy Mater.* 5 (1981) 205.
- [20] D. Elwell, G.M. Rao, *J. Appl. Electrochem.* 18 (1) (1988) 15.
- [21] N. Ibl, J.C. Puipe, H. Angerer, *Surf. Technol.* 6 (4) (1978) 287.
- [22] J.C. Puipe, *Dissertation, ETH, Zürich, Switzerland* (1978).
- [23] P. Chamelot, P. Taxil, D. Oquab, J. Serp, B. Lafage, *J. Electrochem. Soc.* 147 (2000) 4131.
- [24] K. Yasuda, T. Nohira, R. Hagiwara, Y. Ogata, *Electrochim. Acta* 53 (2007) 106.
- [25] K. Kobayashi, T. Nohira, R. Hagiwara, K. Ichitsubo, K. Yamada, *ECS Trans.* 33 (7) (2010) 239.
- [26] G.M. Rao, D. Elwell, R.S. Feigelson, *J. Electrochem. Soc.* 128 (8) (1981) 1708.
- [27] D. Borivent, J. Paret, B. Billia, *J. Phase Equilib. Diff.* 27 (6) (2006) 561.
- [28] K.N. Tu, G. Ottaviana, H. Föll, *J. Appl. Phys.* 54 (2) (1983) 758.
- [29] P.Y. Chevalier, *Thermochim. Acta* 130 (1988) 33.
- [30] G.M. Rao, D. Elwell, R.S. Feigelson, *Surf. Technol.* 13 (1981) 331.